



Prolonged warming of the Brazil Current precedes deglaciations



Thiago P. Santos^a, Douglas O. Lessa^a, Igor M. Venancio^b, Cristiano M. Chiessi^c, Stefan Mulitza^b, Henning Kuhnert^b, Aline Govin^d, Thiago Machado^a, Karen B. Costa^e, Felipe Toledo^e, Bruna B. Dias^a, Ana Luiza S. Albuquerque^{a,*}

^a Departamento de Geoquímica, Universidade Federal Fluminense, Niterói, Brazil

^b MARUM – Center for Marine Environmental Sciences, University of Bremen, Bremen, Germany

^c Escola de Artes, Ciências e Humanidades, Universidade de São Paulo, São Paulo, Brazil

^d Institut Pierre-Simon Laplace/Laboratoire des Sciences du Climat et de l'Environnement, CEA-CNRS-UVSQ, Université Paris Saclay, Gif-sur-Yvette, France

^e Laboratório de Paleoceanografia do Atlântico Sul, Instituto Oceanográfico, Universidade de São Paulo, Brazil

ARTICLE INFO

Article history:

Received 2 July 2016

Received in revised form 6 January 2017

Accepted 15 January 2017

Available online xxxx

Editor: M. Frank

Keywords:

South Atlantic early warming
South Atlantic glacial–interglacial transition
South Atlantic subtropical gyre
low-latitude heat and salt accumulation
interhemispheric heat transfer

ABSTRACT

Paleoceanographic reconstructions from the Brazil Current are scarce and lack the required temporal resolution to appropriately represent its variability during key periods of the last glacial–interglacial cycles. Here, we present the first high-temporal resolution multiproxy reconstruction of the Brazil Current at 24°S covering the last 185 ka. During the last and penultimate glacial periods, our Mg/Ca-derived sea surface temperature (SST) record shows a strong cooling at ca. 47 and ca. 156 ka, respectively, that is followed by a warming trend from late-Marine Isotope Stage (MIS) 3 to MIS 1 and from late-MIS 6 to MIS5e, respectively. Importantly, the Brazil Current warmed uninterrupted towards Termination I (II) after the low SST at ca. 47 and ca. 156 ka, with no SST minima during the Last Glacial Maximum or penultimate glacial maximum. The reason for the strong cooling and the warming trend during late-MIS 3 and late-MIS 6 could reside in the favorable obliquity configuration. However, this mechanism is not sufficient to sustain the warming observed for the rest of the last and penultimate glacial periods. We propose that the change in the Atlantic meridional overturning circulation (AMOC), as described in the literature, from a “warm” to a “cold mode” for MIS 2 and MIS 6 is responsible for the accumulation of warm waters in the subtropical western South Atlantic, preventing SST minima during the last and penultimate glacial maxima in the region. Change in benthic $\delta^{13}\text{C}$ corroborates that a fundamental modification in the AMOC mode might have triggered the heat accumulation. Our data also show a sudden increase in SST and surface salinity during the last glacial descent (MIS 4), indicating that the western portion of the subtropical gyres may have acted as a heat and salt reservoir, while higher latitude climates transitioned to a glacial background. Our findings imply that the AMOC “cold mode” induces heat storage in the subtropical western South Atlantic and, because of that, the last two regional SST minima occurred out-of-phase with the glacial maxima of higher latitudes.

© 2017 Elsevier B.V. All rights reserved.

1. Introduction

The ultimate pacing of glacial–interglacial variations is linked to cyclic changes in the Earth's orbital parameters, but orbital variations are insufficient to drive the large amplitude of climatic cycles (Sigman and Boyle, 2000). Internal feedback mechanisms such as atmospheric CO₂ concentrations, the growth and decay of continental ice sheets and the meridional circulation must amplify the climate response to orbital forcing. In order to better explain the role of each internal mechanism it is fundamental to determine

the timing when the distinct natural archives initiated their transition to a subsequent climate pattern. For the South Atlantic and Southern Ocean, available time series indicate that their altered sea surface temperature (SST) precedes North Atlantic SST warming and ice-volume decay at all orbital frequencies by thousands of years (Mulitza et al., 2007). However, the underlying mechanisms for this remain poorly understood, mainly in southern subtropical gyres. Paleoceanographic studies in subtropical regions, therefore, are crucial to accurately determine the causes of this early response and its possible consequences, since low-latitude oceans provide heat and moisture to high latitudes.

In the South Atlantic subtropical gyre, the western branch is dominated by the Brazil Current (BC). Millennial-scale paleocean-

* Corresponding author.

E-mail address: ana_albuquerque@id.uff.br (A.L.S. Albuquerque).

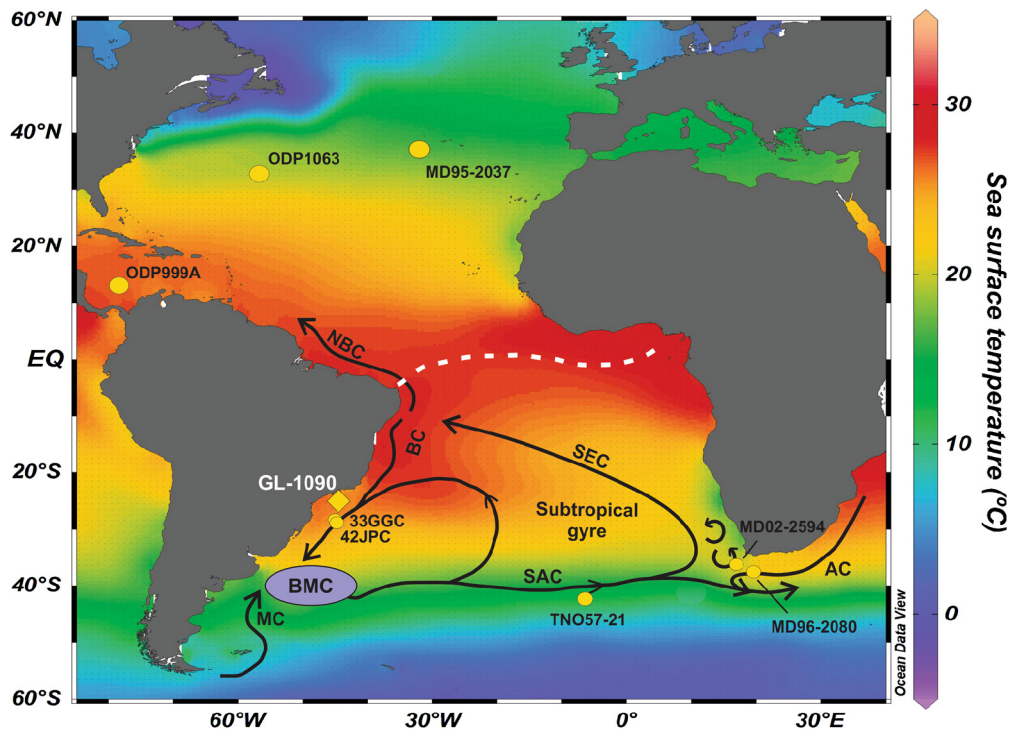


Fig. 1. Position of core GL-1090 (this study) and other records discussed in this work. 33GGC (2082 m) and 42JPC (2500 m) (Tessin and Lund, 2013), TNO57-21 (4981 m) (Barker and Diz, 2014), Agulhas Bank Splice (ABS) formed by the cores MD96-2080 (2488 m) and MD02-2594 (2440 m) (Martínez-Méndez et al., 2010), ODP999A (2827 m) (Schmidt and Spero, 2011), ODP1063 (4584 m) (Böhm et al., 2015), and MD95-2037 (Calvo et al., 2001). Thick black lines represent the main surface currents of interest. AC: Agulhas Current, BC: Brazil Current, MC: Malvinas Current, NBC: North Brazil Current, SAC: South Atlantic Current and SEC: South Equatorial Current. The purple ellipse indicates the region of the Brazil–Malvinas Confluence (BMC). Dashed white line shows the austral summer mean position of Intertropical Convergence Zone (ITCZ). (For interpretation of the reference to color in this figure, the reader is referred to the web version of this article.)

graphic reconstructions show that the southward-flowing BC may have stored and redirected part of the excess heat and salt of the South Atlantic during periods of reduced Atlantic meridional overturning circulation (AMOC) (e.g., Carlson et al., 2008). Such periods, like Heinrich stadial (HS) 1, led to a warming of the surface layer in the BC (e.g. Chiessi et al., 2015). Moreover, benthic foraminifera $\delta^{13}\text{C}$ reveals that the deep Brazil margin received an input of carbon from a ^{13}C -depleted reservoir during HS 1 (Tessin and Lund, 2013). These findings show that shifts in the SST might be coeval with changes in mid-depth ocean ventilation. The association between ocean interior circulation and surface temperature proxies in a long subtropical record could provide important information about climate transitions and reveal the role of ocean circulation in driving subtropical warming.

Here, we present a high-temporal resolution paleoceanographic reconstruction of the subtropical western South Atlantic for the last two glacial cycles. Our results show that the BC SST record fits into the subtropical southern hemisphere pattern described by Pahnke and Sachs (2006), whereby a strong cooling around 47 ka is followed by a warming trend during late-MIS 3. Nonetheless, the warming trend initiated in late-MIS 3 evolved uninterrupted towards Termination I, with no temperature minimum observed during the Last Glacial Maximum (LGM). This feature led to a substantial early warming trend, which also took place during the penultimate glacial (MIS 6). Furthermore, during the last glacial inception (MIS 4), our SST and salinity records demonstrate a sudden transition to a warmer and saltier period that lasted for 10 ka. Together with other studies, we show that MIS 4 was not a period of globally in-phase cold conditions as previously thought. In this way, our findings shed light on the mechanisms responsible for subtropical South Atlantic warming at the end and onset of glacial stages.

2. Study area

The uppermost circulation (0–600 m) in the subtropical western South Atlantic is dominated by the southward-flowing BC (Stramma and England, 1999). The BC originates at ca. 10°S from the southern branch of the bifurcation of the South Equatorial Current that is also the source of the northward-flowing North Brazil Current (Peterson and Stramma, 1991) (Fig. 1). The BC shows its highest intensity during austral spring and summer when the Intertropical Convergence Zone (ITCZ) shifts southward and the northeasterly trade-winds are stronger (Rodrigues et al., 2007). Due to the high incoming solar radiation and excess evaporation that characterize the tropical South Atlantic, the BC at the surface is composed of warm ($>20^\circ\text{C}$) and saline (>36) Tropical Water. Around 38°S , the BC collides with the northward-flowing Malvinas Current, producing the Brazil–Malvinas Confluence (Fig. 1). Most of the South Atlantic Central Water is formed at the Brazil–Malvinas Confluence (Peterson and Stramma, 1991). The South Atlantic Central Water is colder (~ 6 – 20°C), less saline (34.6–36) and richer in nutrients than the Tropical Water. South Atlantic Central Water is then incorporated into the permanent thermocline of the South Atlantic subtropical gyre (Peterson and Stramma, 1991), which is transported southwards by the BC below the Tropical Water at our study site. Deeper in the water column, the western South Atlantic is bathed by the upper portion of the North Atlantic Deep Water (NADW), originating from the northern North Atlantic and circulating between 1200 m and 2500 m (Stramma and England, 1999).

3. Material and methods

3.1. GL-1090 sampling

Core GL-1090 was collected by the Petrobras oil company in the western South Atlantic (24.92°S , 42.51°W , 2225 m water depth,

1914 cm long) (Fig. 1). The core was sampled at approximately 2 cm resolution. GL-1090 consists mostly of greenish to olive glacial sediments somewhat rich in foraminifera-bearing silty clay. Carbonate-rich Holocene and Last Interglacial sediments are represented by more reddish-brown and whitish clays, respectively. From each sample, 10 cm³ of sediment was wet-sieved over a 150- μ m mesh. The residual material was oven-dried for 24 h at 50 °C. The dried material was handpicked with a stereomicroscope to select ideal shells of benthic and planktonic foraminifera for the geochemical analysis described below.

3.2. Oxygen and carbon isotopic composition of planktonic and benthic foraminifera

Benthic foraminifera oxygen ($\delta^{18}\text{O}$) and carbon ($\delta^{13}\text{C}$) stable isotope analyses were performed on 438 samples. In most cases (373 samples), analyses were conducted on the species *Cibicides wuellerstorfi* (250–300 μ m size fraction). For those samples with insufficient *C. wuellerstorfi* (65 samples), we employed the species *Uvigerina peregrina* (250–300 μ m). Planktonic foraminifera analyses were conducted on 832 samples of the species *Globigerinoides ruber* (white variety, *sensu stricto*, 250–300 μ m). For both benthic and planktonic foraminifera samples, around ten shells of each species were selected. The *C. wuellerstorfi* $\delta^{18}\text{O}$ measurements were converted to *U. peregrina* $\delta^{18}\text{O}$ by adding 0.69‰, according to the offset proposed by Zahn et al. (1986). $\delta^{13}\text{C}$ values of the endobenthic *U. peregrina* were not considered. All analyses were performed at the MARUM – Center for Marine Environmental Sciences, University of Bremen, Germany using a Finnigan MAT251 gas isotope ratio mass spectrometer coupled to a Kiel III automated carbonate preparation device. Data were calibrated against an in-house standard (Solnhofen limestone). The results are reported in per mil (‰, parts per thousand) versus Vienna Pee Dee belemnite (VPDB). The standard deviation based on replicate measurements of the in-house standard was 0.06‰ and 0.04‰, for $\delta^{18}\text{O}$ and $\delta^{13}\text{C}$, respectively.

3.3. Planktonic foraminifera Mg/Ca and ice volume-free seawater oxygen isotopic composition

Mg/Ca analyses were performed on samples comprising 30 shells of *G. ruber* (white, *sensu stricto*, 250–300 μ m) that were gently crushed and cleaned following the procedure described by Barker et al. (2003). Before dilution, samples were centrifuged for 10 min to exclude any remaining insoluble particles from the analyses. The diluted solutions were analyzed with an ICP-OES Agilent Technologies 700 Series with an autosampler (ASX-520 Cetac) and a micro-nebulizer at MARUM. After every five samples, instrumental precision was monitored by analyzing an in-house standard solution of 2.93 mmol/mol Mg/Ca. Each Mg/Ca estimate is an average of three replicate analyses. Standards and replicate runs showed a mean reproducibility of ± 0.03 mmol/mol (0.07%). Only samples with Al/Ca < 0.5 μ mol/mol were used, resulting in 606 samples. To convert Mg/Ca ratios into SST, we applied the *G. ruber* calibration [$\text{Mg/Ca} = 0.38 \exp(0.09 \cdot (\text{SST} - 0.61))$] from Dekens (2002) for records shallower than 2.8 km.

The temperature– $\delta^{18}\text{O}$ relationship for *G. ruber* (white) [$\text{SST} = 14.2 - 4.44(\delta^{18}\text{O}_c - \delta^{18}\text{O}_{\text{SW}})$] from Mulitza et al. (2003) was employed to estimate the seawater $\delta^{18}\text{O}$ composition ($\delta^{18}\text{O}_{\text{SW}}$) of surface waters. A conversion factor of 0.27‰ was applied to convert the values from VPDB to Vienna Standard Mean Ocean Water (VSMOW) (Hut, 1987). The effect of changes in global sea level was subtracted from $\delta^{18}\text{O}_{\text{SW}}$ by applying the sea level correction of Waelbroeck et al. (2002) between 185 and 150 ka and Grant et al. (2012) for the last 150 ka. This produced an ice volume-free seawater oxygen isotopic composition ($\delta^{18}\text{O}_{\text{IVF-SW}}$) as a proxy

for changes in sea surface salinity (SSS). $\delta^{18}\text{O}_{\text{IVF-SW}}$ error estimation takes into account an uncertainty of 1.2 °C for the Mg/Ca-SST equation from Dekens (2002), which is equivalent to 0.26‰ $\delta^{18}\text{O}$ change (Mulitza et al., 2003) and an analytical error for $\delta^{18}\text{O}$ of 0.06‰. Hence, the propagated cumulative error estimated for the $\delta^{18}\text{O}_{\text{IVF-SW}}$ was ± 0.27 ‰. Considering the regional $\delta^{18}\text{O}_{\text{SW}}$ SSS relationship proposed by Toledo et al. (2007), our $\delta^{18}\text{O}_{\text{IVF-SW}}$ mostly predicts a fluctuation of 2 salinity units throughout the studied period. Culture experiments have shown a salinity effect on Mg/Ca in the order of 4 salinity units per °C (Dueñas-Bohórquez et al., 2009). Thus, the effect of salinity on our Mg/Ca data would result in an error of 0.5 °C or less. Hönisch et al. (2013) suggest that to a large extent the Mg/Ca salinity sensitivity derived from Atlantic core-top sediments is not a direct effect of salinity, but rather the result of the dissolution correction often applied to Mg/Ca data, which can lead to significant overestimation of temperatures. Therefore, we consider that salinity plays a minor role on the control of Mg incorporation in GL-1090 *G. ruber*.

3.4. Age model

The chronology of core GL-1090 was obtained through the combination of AMS ¹⁴C ages and benthic foraminifera $\delta^{18}\text{O}$ tie-points aligned to two reference curves (Lisiecki and Raymo, 2005; Govin et al., 2014). The complete age–depth model (Fig. 2) was built within the software Bacon v. 2.2, which uses Bayesian statistics to reconstruct Bayesian accumulation histories for sedimentary deposits (Blaauw and Christen, 2011). For the first 327 cm, we selected ten samples for AMS ¹⁴C dating (Supplementary material Table 1). Each sample was composed of about 500 tests of *G. ruber* (white), which were collected from the residue of the >150 μ m mesh after wet sieving and oven drying. The AMS ¹⁴C ages were performed at BETA Analytic (Miami, USA). The ¹⁴C ages were calibrated with the curve Marine13 (Reimer et al., 2013) applying a reservoir age effect of 407 \pm 59 yrs and a ΔR of 7 \pm 59 (Angulo et al., 2007). A reversal was identified at 327 cm (Supplementary material Table 1). Blaauw and Christen (2011) explain that Bacon v. 2.2 is not affected by outlying dates, since the dates are modeled using a Student *t* distribution with wide tails, thereby making the chronological modelling process much more robust against outlying dates. Despite this, we observed that our model presents an improved chronological fit around the negative excursion of benthic $\delta^{13}\text{C}$ related to HS 5 without this reversal. Therefore, the final age-model (Fig. 2) does not consider the reversal at 327 cm. The age–depth model for the interval covered by calibrated ¹⁴C ages is shown in Supplementary material Fig. 1. Between 327 cm and 1914 cm, the chronology was determined by benthic $\delta^{18}\text{O}$ correlation (Fig. 2A–C and Supplementary material Table 2). A plot of the raw benthic $\delta^{18}\text{O}$ records of *C. wuellerstorfi* and *U. peregrina* with the LR04 stack is shown in Supplementary material Fig. 2. The offset between *C. wuellerstorfi* and *U. peregrina* varies at this location, from 0.7‰ during MIS 6 and MIS 4 to almost no offset during MIS 5a (the intervals where *U. peregrina* had to be used). Despite this, there is no temporal difference in the $\delta^{18}\text{O}$ shift of these species, thus not compromising our age-model approach (Supplementary material Fig. 2). The section from 327 cm to 1578 cm was correlated to core MD95-2042, whose chronology has been modified by Govin et al. (2014) using the most recent AICC2012 ice core chronology (Bazin et al., 2013; Veres et al., 2013). This record was used as a reference because of its higher temporal resolution for the last 135 ka, which results in reduced age uncertainties when defining the tie-points. The section from 1578 cm to 1914 cm was correlated to the LR04 benthic $\delta^{18}\text{O}$ stack of Lisiecki and Raymo (2005). Error estimations of $\delta^{18}\text{O}$ tie-points take into account the mean resolution of the GL-1090 benthic $\delta^{18}\text{O}$ record around the tie-point depth, the mean resolu-

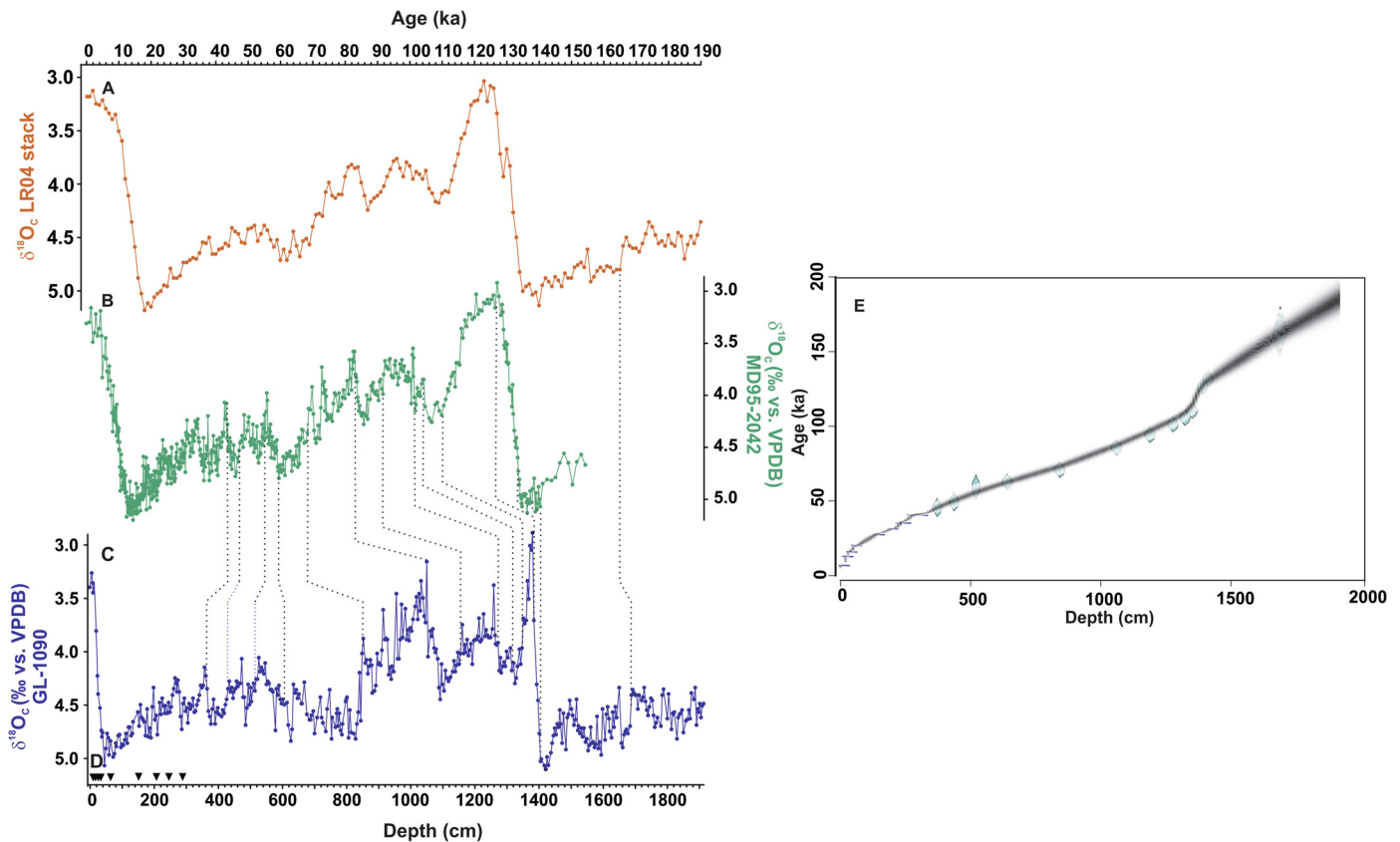


Fig. 2. Reference curves and age–depth model of core GL-1090. A: LR04 benthic foraminifera $\delta^{18}\text{O}$ stack LR04 (Lisiecki and Raymo, 2005). B: MD95-2042 benthic foraminifera $\delta^{18}\text{O}$ plotted with the age–depth model of Govin et al. (2014). C: GL-1090 benthic foraminifera $\delta^{18}\text{O}$. D: GL-1090 calibrated ^{14}C ages. E: Age–depth model based on Bacon v. 2.2 (Blaauw and Christen, 2011). Symbols in panel E represent the positions of calibrated ^{14}C ages and benthic $\delta^{18}\text{O}$ tie-points. Error estimations of $\delta^{18}\text{O}$ tie-points take into account the mean resolution of the GL-1090 benthic $\delta^{18}\text{O}$ record around the tie-point depth, the mean resolution of the reference curve around the tie-point age, a matching error visually estimated when defining tie-points, and the absolute age error of the time-scale used for the reference record.

tion of the reference curve around the tie-point age, a matching error visually estimated when defining the tie-points, and the absolute age error of the time-scale used for the reference record. Beyond the $\delta^{18}\text{O}$ tie-point error estimation, the age model calculated within Bacon v. 2.2 also issues the maximum and minimum error estimation for the interpolation between two consecutive tie-points along the core (Fig. 2E).

According to our age–depth model, core GL-1090 covers the last 185 ka (Fig. 2). Benthic foraminifera $\delta^{18}\text{O}$ presents a well-defined marine isotope stage (MIS) sequence, with lightest values occurring during MIS 5e and MIS 1 (3.0‰ and 3.2‰, respectively). The greatest values of approximately 5.0‰ occurred at the end of MIS 6 and MIS 2. The mean sedimentation rate for the whole core is 13 cm/ka. This provides a mean temporal resolution for the planktonic foraminiferal $\delta^{18}\text{O}$ record of 0.2 ka and for the Mg/Ca and $\delta^{18}\text{O}_{\text{IVF-SW}}$ records of 0.3 ka. The highest resolution period spans from MIS 5c to MIS 2, with an interval between adjacent samples of 0.07 ka during MIS 4 when the sedimentation rate reaches 24 cm/ka. In contrast, MIS 5e, MIS 5d and MIS 1 recorded the lowest temporal resolution, with intervals between adjacent samples reaching 1.2 ka and sedimentation rates as low as 3 cm/ka.

4. Results

4.1. Oxygen and carbon isotopic composition of planktonic and benthic foraminifera

G. ruber $\delta^{18}\text{O}$ varies between -1.31‰ and 0.95‰ (Fig. 3A). The lowest values occurred during MIS 5e and MIS 1 (-1.24‰ and -1.31‰ , respectively). The highest $\delta^{18}\text{O}$ values of approxi-

mately 0.5‰ occurred around the final portion of glacial MIS 6 and MIS 2, as well as during late MIS 4. The penultimate and last deglaciations recorded the highest amplitudes of $\delta^{18}\text{O}$ change of approximately 2.0‰ and 1.7‰ , respectively. The glacial inception during the MIS 5a/4 transition is represented by an increase of around 0.9‰ in $\delta^{18}\text{O}$ (Fig. 3A).

Benthic $\delta^{13}\text{C}$ varies between -0.6‰ and 1.4‰ (Fig. 3D). Long-term negative excursions (as large as 0.8‰) occurred during the latter parts of the penultimate and last glacials, from ca. 150 ka and 40 ka, respectively, as well as during the descent into the last glaciation of MIS 4 when $\delta^{13}\text{C}$ was lower than 0.2‰ . Low benthic $\delta^{13}\text{C}$ values are also present during the MIS 5d/5c and MIS 5b/5a transitions, but these excursions were of shorter duration. The highest $\delta^{13}\text{C}$ values of around 1.0‰ or even higher occurred during MIS 5e, 5c and 5a and MIS 3 and MIS 2 (Fig. 3D).

4.2. Sea surface temperature and ice volume-free seawater oxygen isotopic composition

The mean SST for core GL-1090 was 25.6°C (Fig. 3B). During the last glacial, the lowest SST value (24°C) occurred at ca. 47–45 ka. After 45 ka, SST abruptly increased by 2°C and remained relatively stable until ca. 32 ka, when a new and more gradual warming initiated (Fig. 3B). This warming trend remained constant from late-MIS 3 towards the last deglaciation, elevating the SST by 1°C . At the MIS 2/1 transition, the SST increased by another 1°C . After the strong cooling at 47–45 ka, the SST in the region was raised by about 4°C until the early-Holocene. Other SST minima occurred earlier at mid-MIS 6 (ca. 156 ka), MIS 5b and the MIS 5a/4 transition. Similar to the SST evolution observed during the last glacial,

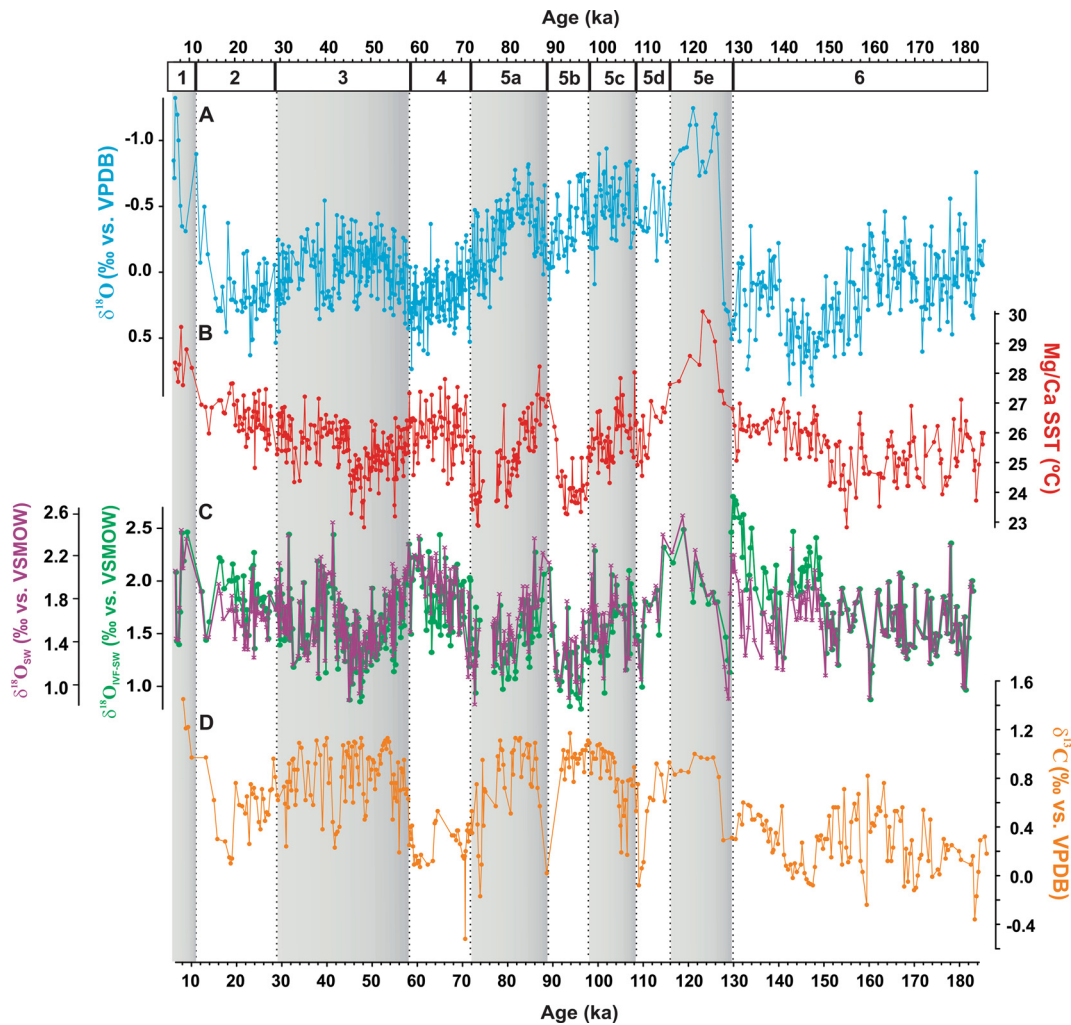


Fig. 3. Main results from core GL-1090. A: *Globigerinoides ruber* $\delta^{18}\text{O}$. B: *G. ruber* Mg/Ca sea surface temperature (SST) ($^{\circ}\text{C}$) applying the calibration equation of Dekens (2002) for *G. ruber* (white). C: $\delta^{18}\text{O}_{\text{IVF-SW}}$ reconstructed with *G. ruber* $\delta^{18}\text{O}$ and Mg/Ca SST ($^{\circ}\text{C}$). Green line is the $\delta^{18}\text{O}_{\text{SW}}$ with ice-volume correction and purple line is the $\delta^{18}\text{O}_{\text{SW}}$ without ice-volume correction. D: *Cibicides wuellerstorfi* $\delta^{13}\text{C}$ (*Uvigerina peregrina* $\delta^{13}\text{C}$ was not considered for the $\delta^{13}\text{C}$ record). Grey bars highlight warm marine isotopic stages. (For interpretation of the references to color in this figure, the reader is referred to the web version of this article.)

cooling during mid-MIS 6 was also followed by a gradual and constant warming trend that was initiated prior to the penultimate deglaciation (Fig. 3B). After this long-term warming, the highest SST values (ca. 30°C) were recorded during the last interglacial (MIS 5e). The last glacial inception between 70 and 60 ka was marked by a strong increase in SST after the low values recorded at the end of substage MIS 5a.

Changes in $\delta^{18}\text{O}_{\text{IVF-SW}}$ were similar to those registered by the SST record, with high variability within MIS 6 (Fig. 3C). The highest $\delta^{18}\text{O}_{\text{IVF-SW}}$ values, corresponding to the highest surface water salinity, were identified during the warm intervals MIS 5e, MIS 5c, MIS 5a and MIS 1, but also during MIS 4 and at the end of the penultimate glacial (MIS 6) (Termination II) (Fig. 3D). All fluctuations in SST and $\delta^{18}\text{O}_{\text{IVF-SW}}$ discussed below are larger than the associated methodological uncertainties.

5. Discussion

5.1. The “low/mid-latitude temperature signal” and early surface warming at the end of the last glacial cycle

The last glacial portion of our SST record is similar to what Pahnke and Sachs (2006) describe as a “low/mid-latitude temperature signal”. This signal is formed by a substantial cooling at ca.

47 ka followed by a warming trend until ca. 23 ka (Pahnke and Sachs, 2006). The good agreement of GL-1090 SST to the compilation shown in Pahnke and Sachs (2006) demonstrates that our record is unlikely to reflect local SST patterns, but, in fact, presents a characteristic signal of subtropical latitudes (Fig. 4).

According to Pahnke and Sachs (2006), the subtropical cooling at ca. 47 ka and the progressive warming that followed was caused by orbital forcing, leading to changes in insolation. The high obliquity at 47 ka resulted in decreased mean annual insolation in subtropical regions between 43°N/S and may have had a significant impact on decreased surface layer temperature, as the upper ocean integrates the mean annual insolation changes over several years (Fig. 4A). Moreover, the eccentricity minimum at this time boosted the contribution of obliquity-driven changes by dampening the precessional amplitude (Pahnke and Sachs, 2006). The GL-1090 SST cooling between 47–45 ka and the subsequent warming was probably controlled by a similar mechanism. The main difference between our reconstruction and the pattern postulated by Pahnke and Sachs (2006) is the absence of a clear temperature minimum around the LGM (23–19 ka) (Fig. 4A–C). Thus, a very early warming trend starting thousands of years prior to the last deglaciation dominated the temperature evolution of the subtropical portion of the BC. The spliced Agulhas Bank (ABS) (cores MD95-2080 and MD02-2594) record (Martínez-Méndez et al., 2010) also presents a

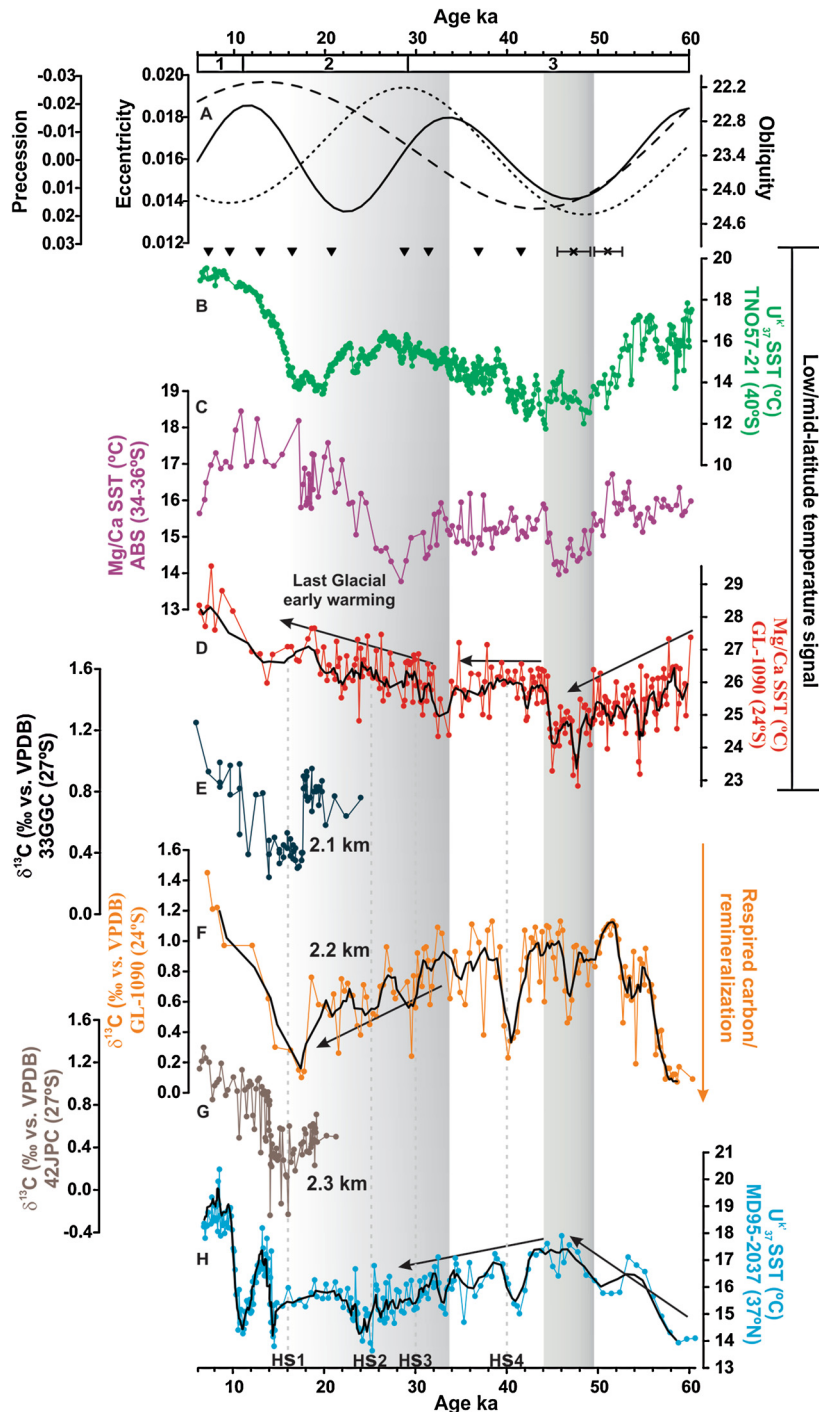


Fig. 4. The “low/mid-latitude temperature signal” and the state of mid-depth ocean ventilation and orbital configuration during the last glacial. A: Precession (thick black line), obliquity (short dashed line) and eccentricity (long dashed line). B: Alkenone-derived sea surface temperature (SST) of TN057-21 (40°S) (Pahnke and Sachs, 2006). C: *Globigerina bulloides* Mg/Ca-derived SST for the Agulhas Bank Splice (ABS) formed by cores MD96-2080 and MD02-2594 (34–36°S) (Martínez-Méndez et al., 2010). D: *Globigerinoides ruber* Mg/Ca-derived SST of GL-1090 (this study). E: *Cibicides* $\delta^{13}\text{C}$ of core 33GGC (Tessin and Lund, 2013). F: *Cibicides wuellerstorfi* $\delta^{13}\text{C}$ of core GL-1090 (this study). G: *Cibicides* $\delta^{13}\text{C}$ of core 42JPC (Tessin and Lund, 2013). H: Alkenone-derived SST of core MD95-2037 (Calvo et al., 2001). Grey bars indicate the strong cooling during MIS 3 and the early warming trend in the southern subtropical records for the last glacial. Black triangles position the calibrated ^{14}C ages and black crosses depict the benthic $\delta^{18}\text{O}$ tie-points used to construct the age–depth model of GL-1090.

Mg/Ca-derived SST pattern similar to the “low/mid-latitude temperature signal”. Their reconstruction shows an early warming trend starting ~ 3 kyr after GL-1090 warming, but still thousands of years prior to the last deglaciation. The same pattern is present in the alkenone-derived SST of Pahnke and Sachs (2006), where the cooling during MIS 3 is more pronounced than the one that occurred during the LGM, i.e. the period with the largest sea and continental ice volume of the last glacial period. These pieces of

evidence indicate that the minimum SST in southern subtropical latitudes could have occurred considerably out-of-phase with glacial maxima of higher latitudes. Therefore, the decrease in obliquity between ~ 45 and 29 ka could be responsible for the increase in mean annual insolation in the subtropics, increasing the SST during late-MIS 3 after the strong cooling at ca. 47–45 ka. With the same reasoning, the increased obliquity from 29 ka on should have led to a decrease in subtropical mean annual insolation, de-

creasing the SST during MIS 2. However, this is not the case, as we observe a SST increase until about 16 ka. Orbital forcing cannot explain the sustained warming through the remaining glacial cycle and another mechanism is necessary to explain the persistent SST increase (Fig. 4A). Based on this, we further explored the potential of internal climate mechanisms related to AMOC interhemispheric heat distribution and mid-depth ventilation to explain the progressive warming occurring after ca. 45 ka and the absence of a SST minimum during the LGM in core GL-1090.

Here, we adopted the definition presented by Böhm et al. (2015) for core ODP1063 (Bermuda Rise) to classify the different AMOC conditions throughout the Last Glacial cycle. In this work, the AMOC “warm mode” concerns the full activity of deep water convection in the high latitude North Atlantic, when the NADW deeply fills the North Atlantic and recirculates near depths of 3 km towards Antarctica. The AMOC “off mode” describes the complete shutdown of the NADW convection and is restricted to some strong abrupt stadial events (Böhm et al., 2015). Finally, the AMOC “cold mode” is an intermediary between the “warm” and “off” modes, and defines the state when sea-ice is sufficiently extensive to affect deep water convection, but the NADW continues recirculating in the top 2 km (Böhm et al., 2015).

Nutrient-related proxies, like benthic $\delta^{13}\text{C}$, are useful tools to investigate changes in deep water circulation. However, the $\delta^{13}\text{C}$ signal can be severely biased by changes in the end-members of source water masses and the addition of respired organic carbon due to biological processes along the advection pathway (Oppo et al., 2015). Terrestrial carbon uptake also has the capacity to alter seawater $\delta^{13}\text{C}$ (Hoogakker et al., 2016). Application of the LGM $\delta^{13}\text{C}$ end-members of Curry and Oppo (2005) to our mean LGM $\delta^{13}\text{C}$ value indicates a 44% contribution of northern component waters against a 56% contribution of Antarctic Bottom Water. During HS 1, this contribution would be even smaller because of the abrupt $\delta^{13}\text{C}$ decrease at ~ 18 ka. Comparison of our data with the values found further south by Tessin and Lund (2013) (Fig. 4E–G) for cores 33GGC and 42JPC suggests that the depletion in benthic $\delta^{13}\text{C}$ during HS 1 is larger by about 0.2‰ each 100 m between 2.1 km and 2.3 km.

LGM GL-1090 foraminifera- ϵ_{Nd} (not affected by carbon cycle dynamics) suggests that bottom waters at the core site were formed by 78% of northern component waters (Howe et al., 2016). For the Holocene, $\delta^{13}\text{C}$ and foraminifera- ϵ_{Nd} indicate very similar proportions of the northern component water of 94 and 93%, respectively. Furthermore, other LGM ϵ_{Nd} results across the Atlantic require the presence of Glacial North Atlantic Intermediate Water (GNAIW) in the upper 2.5 km (Howe et al., 2016). Thus, the most likely cause of the strong glacial reduction in $\delta^{13}\text{C}$ in GL-1090 is related to a weakening of the AMOC (“cold mode”) and the accumulation of ^{13}C -depleted carbon in the upper 2.5 km (Lund et al., 2015; Howe et al., 2016). When the AMOC returns to its “warm mode”, the NADW flushes the respired carbon from the mid-depth South Atlantic, and the $\delta^{13}\text{C}$ and ϵ_{Nd} are again in good agreement.

Under an AMOC “cold mode” scenario, it is expected that the southern hemisphere would trap warm waters mostly in the first 1000 m of the water column (Stocker and Johnsen, 2003). The warming trend initiated during late-MIS 3 was accompanied by a long-term reduction in benthic $\delta^{13}\text{C}$, which culminated in the extremely depleted values during HS 1 (Fig. 4D and F). The progressive AMOC slowdown highlighted by decreasing benthic $\delta^{13}\text{C}$ suggests a reduced efficiency in heat and salt transport from the South to the North Atlantic. Likely, these conditions sustained the surface warming trend observed at the GL-1090 location (Fig. 4A, D and F).

This configuration could also explain the absence of a clear SST minimum during the LGM at our study site (Fig. 4D). Previous works that provide SST reconstructions from the subtropical west-

ern South Atlantic suggested a surface warming from the LGM to HS 1 of around 1 °C (e.g. Carlson et al., 2008; Chiessi et al., 2015). Despite the lower temporal resolution for this interval, GL-1090 also exhibits a temperature increase slightly lower than 1 °C during the LGM/HS 1 transition. However, considering our data, it is difficult to affirm that this small warming was the consequence of reduced AMOC during HS 1 (Fig. 4D). In our view, the HS 1 warming is the result of heat accumulation in the surface ocean throughout late-MIS 3/2, which is coeval with the progressive depletion of benthic $\delta^{13}\text{C}$ caused by the sluggish overturning cell. Interestingly, other earlier HS (HS 6–2), which are better defined in our record, are not characterized by significant SST changes (Fig. 4D). Therefore, our data suggest that millennial-scale events play a marginal role in the SST evolution of the western subtropical South Atlantic, and the long-term trend dominates the variability of the surface ocean in this region. Despite this, rapid negative excursions are present in the benthic $\delta^{13}\text{C}$, especially during HS 4 (Fig. 4D). Therefore, HS represent intervals when mid-depth remineralization of organic carbon was abruptly stronger and the surface ocean kept its gradual warming trend (Fig. 4D, F).

Despite the damped surface millennial-scale SST variability, our data shows a long-term thermal asynchrony with North Atlantic SST records (Fig. 4D, H) (e.g., Calvo et al., 2001), which is usually associated with abrupt millennial events. A clear opposing SST pattern is present in our record compared to the North Atlantic record from core MD95-2037 (Calvo et al., 2001) (Fig. 4D, H). This opposing long-term trend could relate to the fact that such interhemispheric temperature contrast would not require a total shutdown of the AMOC, and the gradual progression of glacial conditions at high northern latitudes, with advancing sea-ice cover, is sufficient to produce wide reorganizations in ocean heat distribution. A recent model study showed that an unstable AMOC regime is present during glacial conditions (Sévellec and Fedorov, 2015). This unstable mode depends on the North Atlantic sea-ice extent, which can shift the formation site of the GNAIW southwards (Sévellec and Fedorov, 2015). Under this scenario, mid-depth convection of the GNAIW can remain active, as suggested by Howe et al. (2016), but with instabilities that create a thermal contrast across the equator. Thus, the gradual increase of sea-ice in the northern hemisphere during late-MIS 3/2 might have limited the transport of warm waters from the western subtropical South Atlantic and contributed to the >10 kyr-long warming period observed in our record.

In summary, the last glacial GL-1090 SST agrees with the subtropical temperature pattern described by Pahnke and Sachs (2006), in which a strong cooling occurred between 47 and 45 ka. This low temperature interval is likely associated with the glacial maximum conditions in the BC and other southern subtropical regions (Fig. 4B–D). Subsequently, a warming trend dominated the surface layer and preceded by thousands of years the increase in greenhouse gases and the onset of the last deglaciation. From late-MIS 3, this warming is coeval with a decrease in benthic $\delta^{13}\text{C}$ likely due to remineralization of organic matter (Fig. 5), which indicates a fundamental change in AMOC. Therefore, we suggest that the warming of the subtropical western South Atlantic is more influenced by the AMOC state itself rather than other climate forcing. Additionally, the warm water reservoir developed by the subtropical western South Atlantic may have worked as a source of moisture contributing to the growth of the Antarctica ice-sheet, as proposed by ice-core water isotope measurements (Stenni et al., 2004).

5.2. Is the early warming trend a pervasive feature of glacial stages?

The early warming trend in core GL-1090 could be interpreted as a feature related to exclusive boundary conditions for the last glacial period. However, a rather similar pattern occurred during

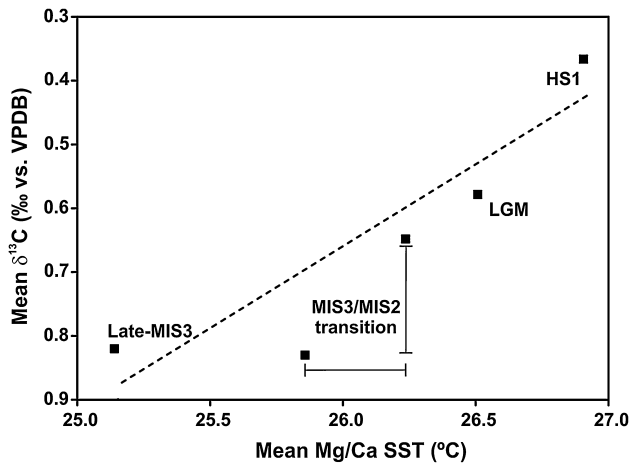


Fig. 5. Mean *Cibicides wuellerstorfi* $\delta^{13}\text{C}$ against mean *Globigerinoides ruber* Mg/Ca-derived SST from the late-MIS 3 towards the Heirinch stadial 1 (HS 1). The MIS3/2 transition records a pronounced shift in benthic $\delta^{13}\text{C}$. After that, the depletion in benthic $\delta^{13}\text{C}$ and the gradual SST increase followed a quasi-linear trend. Dashed-line indicates linear regression.

the latest portion of the penultimate glacial (MIS 6), raising the possibility that this is a pervasive feature present in the western subtropical South Atlantic. Early-MIS 6 (ca. 185–160 ka) is characterized by a much higher SST variability not observed in any part of MIS 3. Subsequently, i.e. between 156 and 152 ka, the coldest temperature for MIS 6 was recorded. The pattern of the SST record here is less prominent than the decreasing trend from 60 ka that culminated in the strong cooling between 47 and 45 ka. Nonetheless, SST during this timeframe achieved values slightly lower than 23 °C, i.e. as cold as the SST minimum of the last glacial period (Fig. 6B).

The distinct pattern of the MIS 3 and MIS 6 SST minima might be related to the totally different orbital configuration. The minimum SST of MIS 6 is coeval with low obliquity and considerably wider precessional amplitude, which could result in stronger insolation and seasonality. Despite the less marked SST minimum, the early warming trend initiated after 152 ka is quite clear and occurred again thousands of years earlier than the Termination II that culminated in the highest SST recorded during the Last Interglacial MIS 5e at 121 ka. Repetition of this glacial early warming was also observed in the spliced Agulhas Bank SST record, where the authors showed a clear increment in the temperature initiated at early-MIS 6, with a steeper evolution after ~ 152 ka (Fig. 6C) (Martínez-Méndez et al., 2010). In that study, SST during the end of the penultimate glacial was even warmer than the temperature of the Last Interglacial (Martínez-Méndez et al., 2010) (Fig. 6C). The authors explained their results for *Globigerina bulloides* Mg/Ca based on the increased influence of Agulhas waters during the winter, and the east-west migration of the Agulhas retroflection.

Our depleted benthic $\delta^{13}\text{C}$ together with Mg/Ca SST could provide an additional explanation. In general, MIS 6 benthic $\delta^{13}\text{C}$ is marked by lower values compared with the Last Glacial. The early- to mid-MIS 6 $\delta^{13}\text{C}$ record is characterized by higher variability, reaching peaks of 0.7‰ (0.3‰ lower than the peaks during MIS 3) (Fig. 6D). From 152 ka (late-MIS 6), the variability decreases and very depleted values of 0.0‰ occurred simultaneously with the onset of surface warming. As the benthic $\delta^{13}\text{C}$ data strongly indicate a connection between mid-depth ocean ventilation and surface heat distribution, the depletion of benthic $\delta^{13}\text{C}$ from late-MIS 6 likely marks the time when the rate of interhemispheric heat transfer slowed down and the residence time of the GNAIV increased (Fig. 6B and D).

The ε_{Nd} record from Bermuda Rise (Fig. 6E) indicates that late-MIS 6 (and also MIS 2) was a period of AMOC “cold mode”

(Böhm et al., 2015). Likely, this “cold mode” is the condition associated with the sustained heat accumulation and depletion of benthic $\delta^{13}\text{C}$ in the western subtropical South Atlantic that triggered an early warming trend during the final portion of the last two glacial cycles. The beginning of an AMOC “cold mode” period inhibits the western subtropical South Atlantic from recording low SST coeval with glacial maxima at higher latitudes. Thus, the SST minima during glacial stages in the BC region should necessarily occur prior to the onset of the “cold mode”, i.e. when the AMOC is still in “warm mode” (Böhm et al., 2015) and the western subtropical South Atlantic is shedding heat towards higher latitudes of the North Atlantic through the subtropical gyre recirculation cell. Therefore, we suggest that, if all recent glacial stages have an AMOC “cold mode”, this would likely result in an early glacial cooling that is immediately followed by an early warming trend in the western subtropical South Atlantic.

5.3. The vigorous Brazil Current during the last glacial descent (MIS 4)

The interval between 60 and 70 ka represents the transition into full glacial conditions. Barker and Diz (2014) suggest that the transition in the Earth’s climate during this period was globally synchronous, generating in-phase cold conditions between southern and northern high latitudes. However, a slightly different picture might emerge as high-temporal resolution records from subtropical latitudes are produced.

In core GL-1090, SST reached ~ 27 °C during substage MIS 5a and then decreased progressively towards the MIS 5a/4 transition (Fig. 7E). However, after 70 ka, SST rose abruptly and achieved values similar to peak conditions during substages MIS 5a and 5c, remaining elevated throughout MIS 4. The explanation for this long and stable warming in our record could reside in the complex combination of (i) shifts associated with the Antarctic Circumpolar Current (ACC) and the entire subtropical gyre, (ii) mid-depth ocean circulation and (iii) orbital configuration.

A temperature record from the SE Pacific suggests that the enhanced cooling during MIS 4 was caused by a 5–6° northward shift of the ACC/subtropical gyre system (Kaiser et al., 2005). This movement of the subtropical gyre and its associated currents would likely affect the position of the SEC bifurcation in the western South Atlantic. A numerical model study observed that seasonal variation at the latitude where the bifurcation is located partially controls the strength of the NBC and the BC (Rodrigues et al., 2007). In this case, if the bifurcation moved northward together with the ACC/subtropical gyre system, transport of the BC would increase at the expense of a reduction in transport of the NBC. Northward displacement of the bifurcation is also favored by a southward movement of the local wind stress of the marine ITCZ (Rodrigues et al., 2007). Tropical rainfall reconstructions indicate a relatively southerly position of the ITCZ between 60 and 70 ka, and even further south when HS 6 was initiated during the final period of MIS 4 (~ 64 ka) (Deplazes et al., 2013). Thus, this period combined optimal conditions for the northernmost position of the SEC bifurcation, strengthening the transport of the BC and increasing SST and salinity over site GL-1090 (Fig. 7E and F). Likely, this mechanism is also active when climate approach the maximum glacial conditions during the end of MIS 2 and MIS 6. Similarly to HS of MIS 3 and 2, it is difficult to identify a specific response of our SST record to HS 6, given that the abrupt temperature increase was initiated clearly prior to the onset of HS 6 (Fig. 7e). The northward movement of the ACC/subtropical gyre also shifts the strong SST gradient formed at the Subtropical Front. This interpretation fits with the observations of Barker and Diz (2014) that called for an enhanced latitudinal temperature gradient within the South Atlantic/Southern Ocean to explain the low values of *G. bulloides* $\delta^{18}\text{O}$ within this interval in core TNO57-21.

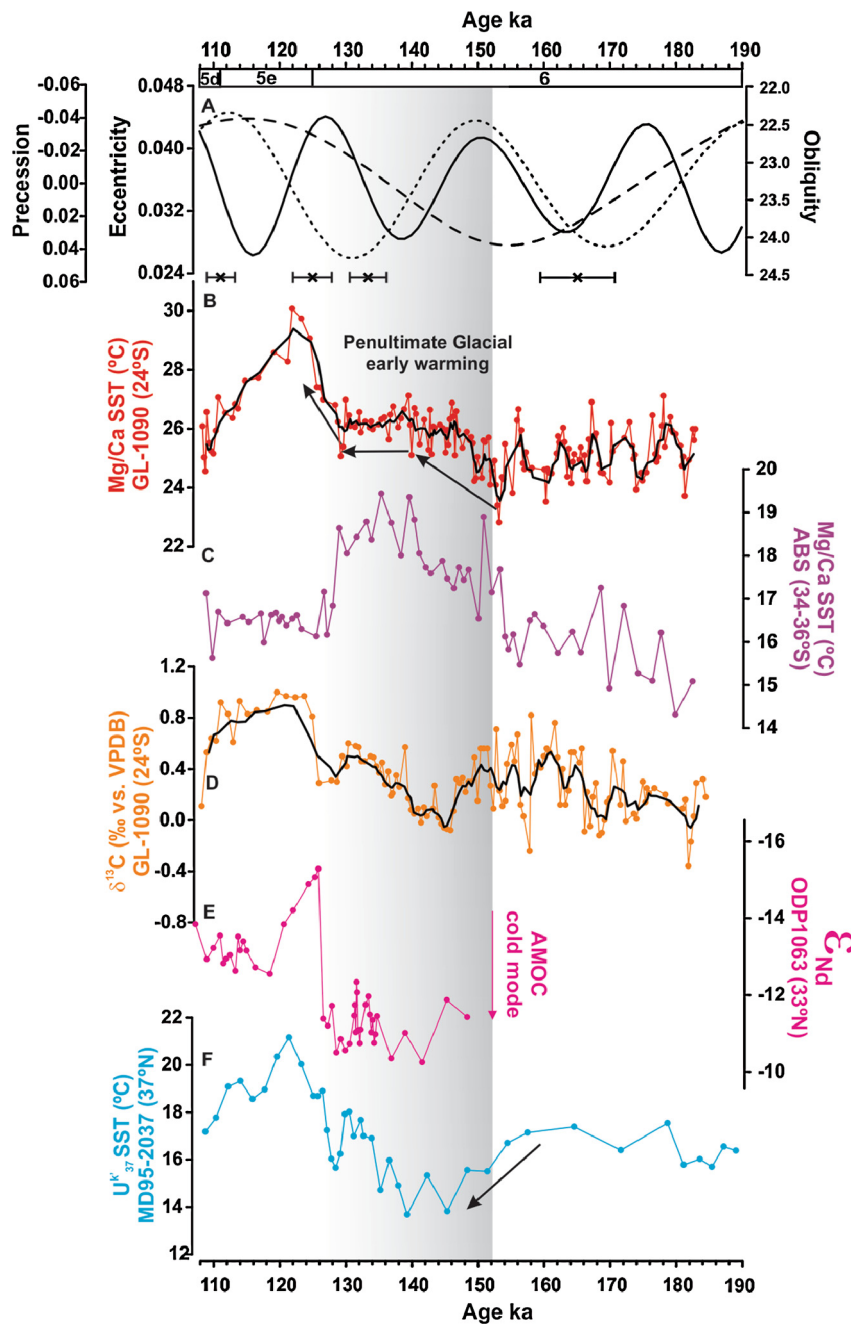


Fig. 6. The state of mid-depth ocean ventilation and orbital configuration during the penultimate glacial A: Precession (thick black line), obliquity (short dashed line) and eccentricity (long dashed line). B: *Globigerinoides ruber* Mg/Ca-derived SST of GL-1090 (this study). C: *Globigerina bulloides* Mg/Ca-derived SST for the Agulhas Bank Splice (ABS) formed by cores MD96-2080 and MD02-2594 (34–36°S) (Martínez-Méndez et al., 2010). D: *Cibicides wuellerstorfi* $\delta^{13}\text{C}$ of core GL-1090 (this study). E: ϵ_{Nd} record of core ODP1063 (Böhm et al., 2015). F: Alkenone-derived SST of core MD95-2037 (Calvo et al., 2001). Grey bar indicates the beginning of early warming trend for the penultimate glacial for the southern subtropical records. Black crosses position the benthic $\delta^{18}\text{O}$ tie-points.

Notably, a warm glacial inception is not an exclusive feature of GL-1090. The Caribbean Sea core ODP999A, despite its lower temporal resolution for this interval, also shows a clear warming trend demonstrated by high Mg/Ca-derived SST during MIS 4 (Fig. 7D) (Schmidt and Spero, 2011). Furthermore, a pronounced thermal gradient between cold air temperatures and a warm subtropical North Atlantic has been proposed as the mechanism for fast ice sheet expansion at this time in Greenland and northern Europe (Sánchez Goñi et al., 2013). This evidence reinforces the argument that the BC, and other subtropical gyre currents, might have stored warm and salty waters during such transitions while the climate system transitioned into a glacial background at higher latitudes (Fig. 7B–H).

Regarding ventilation of the ocean interior, the MIS 5a/4 transition reveals important changes. GL-1090 benthic $\delta^{13}\text{C}$ exhibits an abrupt shift from 70 ka, showing extremely depleted values of 0.1‰ or even lower (Fig. 7I). These values are comparable to those of HS 1, but were produced considerably faster compared with the gradual decrease that occurred from late-MIS 3 up to HS 1 (Fig. 5). Obviously, the same processes potentially affecting HS 1 $\delta^{13}\text{C}$ values (see section 5.1) are also at play during the MIS 5a/4 transition, which could overestimate the shallow flow of the GNAIW. However, MIS 4 is characterized by a period of strong CO_2 sequestration (Bereiter et al., 2012), which requires an expansion of Antarctic Bottom Water to accommodate a larger amount of respired carbon in the deep ocean (Menviel et al., 2012). South-

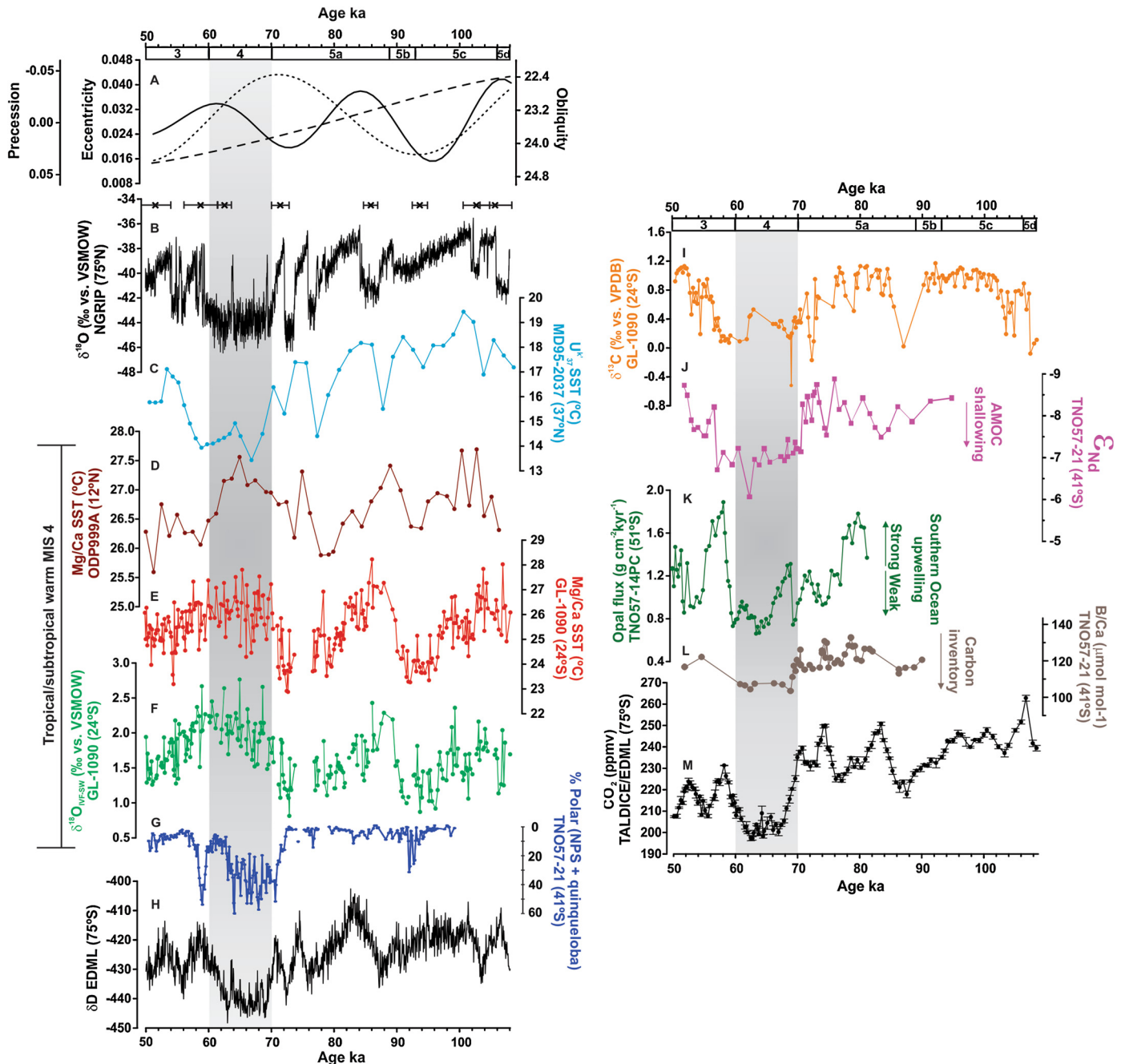


Fig. 7. Comparison of last glacial descent (MIS 4) between low and high latitude records (left hand panel) and state of mid/deep ocean ventilation as well as atmospheric carbon dioxide concentration (right hand panel). A: Precession (thick black line), obliquity (short dashed line) and eccentricity (long dashed line). B: Northern Greenland Ice Core Project $\delta^{18}\text{O}$ (NGRIP Community Members, 2004) plotted on AICC2012 time-scale (Bazin et al., 2013; Veres et al., 2013). C: Alkenone-derived sea surface temperature (SST) of core MD95-2037 (Calvo et al., 2001). D: *Globigerinoides ruber* Mg/Ca-derived SST of ODP999A (Schmidt and Spero, 2011). E: *G. ruber* Mg/Ca-derived SST of GL-1090 (this study). F: $\delta^{18}\text{O}_{\text{IVF-SW}}$ of GL-1090 (this study). G: Relative abundance of *Neoglobobulimina papyderma sinistral* and *Turborotalia quinqueloba* of TNO57-21 (Barker and Diz, 2014). H: Antarctica δD of Dronning Maud Land (Epica Community Members, 2004) plotted on AICC2012 time-scale (Bazin et al., 2013; Veres et al., 2013). I: *Cibicides wuellerstorfi* $\delta^{13}\text{C}$ of core GL-1090 (this study). J: ϵ_{Nd} record of core TNO57-21 (Piotrowski et al., 2005). K: Opal flux of TNO57-13 and TNO57-14 (Anderson et al., 2009). L: B/Ca ratio of core TNO57-21 (Yu et al., 2016). M: Carbon dioxide in TALDICE/EDML ice-cores (Bereiter et al., 2012). Grey bar in the right hand panel indicates the contrasting MIS 4 pattern of low and high latitude. Grey bar in the left hand panel highlights the contrasting MIS 4 pattern of low and high latitude. Black crosses position the benthic $\delta^{18}\text{O}$ tie-points.

ern Atlantic ϵ_{Nd} has shown higher radiogenic values from about -8.3 (late-MIS 5a) to -7.3 (MIS 4), indicating a retraction of the GNAIW (Fig. 7J) (Piotrowski et al., 2005). Opal flux in the Southern Ocean accounts for a rather reduced upwelling in this period, which increases stratification and retains the carbon in deep layers (Fig. 7K) (Anderson et al., 2009). Benthic foraminifera B/Ca ratios indicate that enhanced deep carbon storage by at least 50 Gt reduced the carbonate ion concentration by around $25 \mu\text{mol kg}^{-1}$

during MIS 4 (Fig. 7L) (Yu et al., 2016). This set of findings, combined with the abrupt nature of our benthic $\delta^{13}\text{C}$, may indicate that, at least in part, a shoaling of AMOC could have contributed to the severe $\delta^{13}\text{C}$ depletion (Fig. 7J–N).

Finally, an orbital component may have been associated with the warm MIS 4. During the MIS 5a/4 transition, obliquity changed to very low values, in contrast to what was found for the strong cooling at 47 ka (Fig. 7a). This low obliquity resulted in high

mean annual insolation between 43 °N/S, consequently warming the subtropical surface ocean. Therefore, MIS 4 represented ideal conditions for the establishment of a strong, warm and salty BC. However, more high-temporal resolution records are needed to accurately determine the role of low-latitude subtropical regions in long time-scale transitions and to decouple the factors behind the strong $\delta^{13}\text{C}$ lowering during this period.

6. Conclusions

The western subtropical Atlantic SST record shown in this study for the last glacial period is characterized by a pattern typical for southern mid-latitudes, with a pronounced cooling between 47 and 45 ka. Interestingly, this cooling revealed the lowest temperature for the Brazil Current for the last glacial period. Subsequently, this interval was followed by a gradual early warming trend throughout the late-MIS 3/MIS 2 and, because of that, no minimum SST was recorded during the LGM. The early warming was also a dominant feature during the penultimate glacial, suggesting that this is a pervasive behavior of the western subtropical South Atlantic during glacial stages. Both early warming trends were coeval with depleted benthic $\delta^{13}\text{C}$, indicating that they are linked to mid-depth convection when the AMOC initiated its glacial “cold mode”. When the “cold mode” starts, the western subtropical South Atlantic warms uninterruptedly so that SST minima that are synchronous with conventional glacial maxima at higher latitudes cannot happen. We conclude that the SST minimum in our region during glacial stages should occur necessarily out-of-phase with the glacial maxima at high northern and southern latitudes. Such cold conditions would occur when the AMOC is in its “warm mode” and the western subtropical South Atlantic is releasing heat through its surface currents. Furthermore, together with other MIS 4 SST records, we suggest that the subtropics could have stored warm and salty waters while higher latitude climates transitioned to full glacial conditions.

Acknowledgements

Petrobras provided the sediment core employed in this research. We thank S. Pape and M. Kölling for doing Mg/Ca analysis. S. Barker, C. Charles and R. Kowsman (CENPES/Petrobras) yielded important contributions during manuscript preparation. TPS acknowledges the financial support from CAPES/PDSE (grant 99999.007924/2014-03). ALA is a CNPq senior researcher (grant 306385/2013-9) and thanks them for financial support (grant 99999.002675/2015-03). CMC acknowledges the financial support from FAPESP (grant 2012/17517-3) and CAPES (grant 564/2015). We also thank S. Di Chiara for help during sample preparation. We thank two anonymous reviewers and the Editor for their constructive comments. This study was supported by CAPES/Paleocean project (23038.001417/2914-71). The data reported in this paper will be archived in Pangaea (www.pangaea.de).

Appendix A. Supplementary material

Supplementary material related to this article can be found online at <http://dx.doi.org/10.1016/j.epsl.2017.01.014>.

References

- Anderson, R.F., Ali, S., Bradtmiller, L.I., Nielsen, S.H.H., Fleisher, M.Q., Anderson, B.E., Burckle, L.H., 2009. Wind-driven upwelling in the Southern Ocean and the deglacial rise in atmospheric CO_2 . *Science* 323, 1443–1448. <http://dx.doi.org/10.1126/science.1167441>.
- Angulo, R.J., Reimer, P.J., de Souza, M.C., Sheel-Ybert, R., Tenorio, M.C., Disaro, S.T., Gaspar, M.D., 2007. A tentative determination of upwelling influence on the paleo-surficial marine water reservoir effect in Southeastern Brazil. *Radiocarbon* 49, 1255–1259. <https://doi.org/10.1017/S0033822200043162>.
- Barker, S., Diz, P., 2014. Timing of the descent into the last Ice Age determined by the bipolar seesaw. *Paleoceanography* 29, 489–507. <http://dx.doi.org/10.1002/2014PA002623>.
- Barker, S., Greaves, M., Elderfield, H., 2003. A study of cleaning procedures used for foraminiferal Mg/Ca paleothermometry. *Geochem. Geophys. Geosyst.* 4, 1–20. <http://dx.doi.org/10.1029/2003GC000559>.
- Bazin, L., Landais, A., Lemieux-Dudon, B., Toyé Mahamadou Kele, H., Veres, D., Parrenin, F., Martinerie, P., Ritz, C., Capron, E., Lipenkov, V., Loutre, M.F., Raynaud, D., Vinther, B., Svensson, A., Rasmussen, S.O., Severi, M., Blunier, T., Leuenberger, M., Fischer, H., Masson-Delmotte, V., Chappellaz, J., Wolff, E., 2013. An optimized multi-proxy, multi-site Antarctic ice and gas orbital chronology (AICC2012): 120–800 ka. *Clim. Past* 9, 1715–1731. <http://dx.doi.org/10.5194/cp-9-1715-2013>.
- Bereiter, B., Luthi, D., Siegrist, M., Schupbach, S., Stocker, T.F., Fischer, H., 2012. Mode change of millennial CO_2 variability during the last glacial cycle associated with a bipolar marine carbon seesaw. *Proc. Natl. Acad. Sci.* 109, 9755–9760. <http://dx.doi.org/10.1073/pnas.1204069109>.
- Blaauw, M., Christen, J.A., 2011. Flexible paleoclimate age–depth models using an autoregressive gamma process. *Bayesian Anal.* 6, 457–474. <http://dx.doi.org/10.1214/11-BA618>.
- Böhm, E., Lippold, J., Gutjahr, M., Frank, M., Blaser, P., Antz, B., Fohlmeister, J., Frank, N., Andersen, M.B., Deininger, M., 2015. Strong and deep Atlantic meridional overturning circulation during the last glacial cycle. *Nature* 517, 73–76. <http://dx.doi.org/10.1038/nature14059>.
- Calvo, E., Villanueva, J., Grimalt, J.O., Boelaert, A., Labeyrie, L., 2001. New insights into the glacial latitudinal temperature gradients in the North Atlantic. Results from UK37 sea surface temperatures and terrigenous inputs. *Earth Planet. Sci. Lett.* 188, 509–519. [http://dx.doi.org/10.1016/S0012-821X\(01\)00316-8](http://dx.doi.org/10.1016/S0012-821X(01)00316-8).
- Carlson, A.E., Oppo, D.W., Came, R.E., LeGrande, A.N., Keigwin, L.D., Curry, W.B., 2008. Subtropical Atlantic salinity variability and Atlantic meridional circulation during the last deglaciation. *Geology* 36, 991–994. <http://dx.doi.org/10.1130/G25080A.1>.
- Chiessi, C.M., Mulitza, S., Mollenhauer, G., Silva, J.B., Groeneveld, J., Prange, M., 2015. Thermal evolution of the western South Atlantic and the adjacent continent during Termination 1. *Clim. Past* 11, 915–929. <http://dx.doi.org/10.5194/cp-11-915-2015>.
- Curry, W.B., Oppo, D.W., 2005. Glacial water mass geometry and the distribution of $\delta^{13}\text{C}$ of ΣCO_2 in the western Atlantic Ocean. *Paleoceanography*, 20. <http://dx.doi.org/10.1029/2004PA001021>.
- Dekens, P.S., 2002. Core top calibration of Mg/Ca in tropical foraminifera: refining paleotemperature estimation. *Geochem. Geophys. Geosyst.* 3. <http://dx.doi.org/10.1029/2001GC000200>.
- Deplazes, G., Lückge, A., Peterson, L.C., Timmermann, A., Hamann, Y., Hughen, K.A., Röhl, U., Laj, C., Cane, M.A., Sigman, D.M., Haug, G.H., 2013. Links between tropical rainfall and North Atlantic climate during the last glacial period. *Nat. Geosci.* 6, 1–5. <http://dx.doi.org/10.1038/ngeo1712>.
- Dueñas-Bohórquez, A., da Rocha, R.E., Kuroyanagi, A., Bijma, J., Reichert, G.J., 2009. Effect of salinity and seawater calcite saturation state on Mg and Sr incorporation in cultured planktonic foraminifera. *Mar. Micropaleontol.* 73, 178–189. <http://dx.doi.org/10.1016/j.marmicro.2009.09.002>.
- Epica Community Members, 2004. Eight glacial cycles from an Antarctic ice core. *Nature* 429, 623–628. <http://dx.doi.org/10.1038/nature02599>.
- Govin, A., Chiessi, C.M., Zabel, M., Sawakuchi, A.O., Heslop, D., Hörner, T., Zhang, Y., Mulitza, S., 2014. Terrigenous input off northern South America driven by changes in Amazonian climate and the North Brazil Current retroflection during the last 250 ka. *Clim. Past* 10, 843–862. <http://dx.doi.org/10.5194/cp-10-843-2014>.
- Grant, K.M., Rohling, E.J., Bar-Matthews, M., Ayalon, A., Medina-Elizalde, M., Ramsey, C.B., Satow, C., Roberts, A.P., 2012. Rapid coupling between ice volume and polar temperature over the past 150,000 years. *Nature* 491, 744–747. <http://dx.doi.org/10.1038/nature11593>.
- Hönisch, B., Allen, K.A., Lea, D.W., Spero, H.J., Eggins, S.M., Arbuszewski, J., deMenocal, P., Rosenthal, Y., Russell, A.D., Elderfield, H., 2013. The influence of salinity on Mg/Ca in planktic foraminifera – evidence from cultures, core-top sediments and complementary $\delta^{18}\text{O}$. *Geochim. Cosmochim. Acta* 121, 196–213. <http://dx.doi.org/10.1016/j.gca.2013.07.028>.
- Hoogakker, B.A.A., Smith, R.S., Singarayer, J.S., Marchant, R., Prentice, I.C., Allen, J.R.M., Anderson, R.S., Bhagwat, S.A., Behling, H., Borisova, O., Bush, M., Correa-Metrio, A., De Vernal, A., Finch, J.M., Fréchet, B., Lozano-Garcia, S., Gosling, W.D., Granoszewski, W., Grimm, E.C., Grüger, E., Hanselman, J., Harrison, S.P., Hill, T.R., Huntley, B., Jiménez-Moreno, G., Kershaw, P., Ledru, M.P., Magri, D., McKenzie, M., Müller, U., Nakagawa, T., Novenko, E., Penny, D., Sadori, L., Scott, L., Stevenson, J., Valdes, P.J., Vandergoes, M., Velichko, A., Whitlock, C., Tzedakis, C., 2016. Terrestrial biosphere changes over the last 120 kyr. *Clim. Past* 12, 51–73. <http://dx.doi.org/10.5194/cp-12-51-2016>.
- Howe, J.N.W., Piotrowski, A.M., Noble, T.L., Mulitza, S., Chiessi, C.M., Bayon, G., 2016. North Atlantic deep water production during the last glacial maximum. *Nat. Commun.* 7, 11765. <http://dx.doi.org/10.1038/ncomms11765>.
- Hut, G., 1987. Stable isotope reference samples for geochemical and hydrological investigations. Consultant group meeting IAEA, Vienna 16–18 September 1985, Report to the Director General. International Atomic Energy Agency, Vienna.

- Kaiser, J., Lamy, F., Hebbeln, D., 2005. A 70-kyr sea surface temperature record off southern Chile (Ocean Drilling Program Site 1233). *Paleoceanography* 20, 1–15. <http://dx.doi.org/10.1029/2005PA001146>.
- Lisiecki, L.E., Raymo, M.E., 2005. A Pliocene–Pleistocene stack of 57 globally distributed benthic $\delta^{18}\text{O}$ records. *Paleoceanography* 20, 1–17. <http://dx.doi.org/10.1029/2004PA001071>.
- Lund, D.C., Tessin, A.C., Hoffman, J.L., Schmittner, A., 2015. Southwest Atlantic water mass evolution during the last deglaciation. *Paleoceanography* 30, 477–494. <http://dx.doi.org/10.1002/2014PA002657>.
- Martínez-Méndez, G., Zahn, R., Hall, I.R., Peeters, F.J.C., Pena, L.D., Cacho, I., Nègre, C., 2010. Contrasting multiproxy reconstructions of surface ocean hydrography in the Agulhas Corridor and implications for the Agulhas Leakage during the last 345,000 years. *Paleoceanography* 25, 1–12. <http://dx.doi.org/10.1029/2009PA001879>.
- Menviel, L., Joos, F., Ritz, S.P., 2012. Simulating atmospheric CO_2 , $\delta^{13}\text{C}$ and the marine carbon cycle during the Last Glacial–Interglacial cycle: possible role for a deepening of the mean remineralization depth and an increase in the oceanic nutrient inventory. *Quat. Sci. Rev.* 56, 46–68. <http://dx.doi.org/10.1016/j.quascirev.2012.09.012>.
- Mulitza, S., Boltovskoy, D., Donner, B., Meggers, H., Paul, A., Wefer, G., 2003. Temperature: $\delta^{18}\text{O}$ relationships of planktonic foraminifera collected from surface waters. *Palaeogeogr. Palaeoclimatol. Palaeoecol.* 202, 143–152. [http://dx.doi.org/10.1016/S0031-0182\(03\)00633-3](http://dx.doi.org/10.1016/S0031-0182(03)00633-3).
- Mulitza, S., Paul, A., Wefer, G., 2007. Paleocyanography records/Late Pleistocene South Atlantic. *Encycl. Quat. Sci.*, 1816–1831. <http://dx.doi.org/10.1016/B978-0-444-53643-3.00298-3>.
- NGRIP Community Members, 2004. High-resolution record of Northern Hemisphere climate extending into the last interglacial period. *Nature* 431 (7005), 147–151. <http://dx.doi.org/10.1038/nature02805>.
- Oppo, D.W., Curry, W.B., McManus, J.F., 2015. What do benthic $\delta^{13}\text{C}$ and $\delta^{18}\text{O}$ data tell us about Atlantic circulation during Heinrich Stadial. *Paleoceanography* 30 (4), 353–368. <http://dx.doi.org/10.1002/2014PA002667>.
- Pahnke, K., Sachs, J.P., 2006. Sea surface temperatures of southern midlatitudes 0–160 kyr B.P. *Paleoceanography* 21, 1–17. <http://dx.doi.org/10.1029/2005PA001191>.
- Peterson, R.G., Stramma, L., 1991. Upper-level circulation in the South Atlantic Ocean. *Prog. Oceanogr.* 26, 1–73. [http://dx.doi.org/10.1016/0079-6611\(91\)90006-8](http://dx.doi.org/10.1016/0079-6611(91)90006-8).
- Piotrowski, A.M., Goldstein, S.L., Hemming, S.R., Fairbanks, R.G., 2005. Temporal relationships of carbon cycling and ocean circulation at glacial boundaries. *Science* 307, 1933–1938. <http://dx.doi.org/10.1126/science.1104883>.
- Reimer, P.J., Bard, E., Bayliss, A., Beck, J.W., Blackwell, P.G., Ramsey, C.B., 2013. IntCal13 and Marine13 radiocarbon age calibration curves 0–50,000 years cal BP. *Radiocarbon* 55, 1869–1887. http://dx.doi.org/10.2458/azu_js_rc.55.16947.
- Rodrigues, R.R., Rothstein, L.M., Wimbush, M., 2007. Seasonal variability of the South Equatorial Current Bifurcation in the Atlantic Ocean: a numerical study. *J. Phys. Oceanogr.* 37, 16–30. <http://dx.doi.org/10.1175/JPO2983.1>.
- Sánchez Goñi, M.F., Bard, E., Landais, A., Rossignol, L., D'Errico, F., 2013. Air–sea temperature decoupling in western Europe during the last interglacial–glacial transition. *Nat. Geosci.* 6, 837–841. <http://dx.doi.org/10.1038/ngeo1924>.
- Schmidt, M.W., Spero, H.J., 2011. Meridional shifts in the marine ITCZ and the tropical hydrologic cycle over the last three glacial cycles. *Paleoceanography* 26, 1–15. <http://dx.doi.org/10.1029/2010PA001976>.
- Sévellec, F., Fedorov, A.V., 2015. Unstable AMOC during glacial intervals and millennial variability: the role of mean sea ice extent. *Earth Planet. Sci. Lett.* 429, 60–68. <http://dx.doi.org/10.1016/j.epsl.2015.07.022>.
- Sigman, D.M., Boyle, E.A., 2000. Glacial/interglacial variations in atmospheric carbon dioxide. *Nature* 407, 859–869. <http://dx.doi.org/10.1038/35038000>.
- Stenni, B., Jouzel, J., Masson-Delmotte, V., Röthlisberger, R., Castellano, E., Cattani, O., Falourd, S., Johnsen, S.J., Longinelli, A., Sachs, J.P., Selmo, E., Souchez, R., Steffensen, J.P., Udisti, R., 2004. A late-glacial high-resolution site and source temperature record derived from the EPICA Dome C isotope records (East Antarctica). *Earth Planet. Sci. Lett.* 217, 183–195. [http://dx.doi.org/10.1016/S0012-821X\(03\)00574-0](http://dx.doi.org/10.1016/S0012-821X(03)00574-0).
- Stocker, T.F., Johnsen, S.J., 2003. A minimum thermodynamic model for the bipolar seesaw. *Paleoceanography* 18. <http://dx.doi.org/10.1029/2003PA000920>.
- Stramma, L., England, M., 1999. On the water masses and mean circulation of the South Atlantic Ocean. *J. Geophys. Res., Oceans* 104, 20863–20883. <http://dx.doi.org/10.1029/1999JC900139>.
- Tessin, A.C., Lund, D.C., 2013. Isotopically depleted carbon in the mid-depth South Atlantic during the last deglaciation. *Paleoceanography* 28, 296–306. <http://dx.doi.org/10.1002/palo.20026>.
- Toledo, F.A.L., Costa, K.B., Pivel, M.A.G., 2007. Salinity changes in the western tropical South Atlantic during the last 30 kyr. *Glob. Planet. Change* 57, 383–395. <http://dx.doi.org/10.1016/j.gloplacha.2007.01.001>.
- Veres, D., Bazin, L., Landais, a., Toyé Mahamadou Kele, H., Lemieux-Dudon, B., Parrenin, F., Martinerie, P., Blayo, E., Blunier, T., Capron, E., Chappellaz, J., Rasmussen, S.O., Severi, M., Svensson, a., Vinther, B., Wolff, E.W., 2013. The Antarctic ice core chronology (AICC2012): an optimized multi-parameter and multi-site dating approach for the last 120 thousand years. *Clim. Past* 9, 1733–1748. <http://dx.doi.org/10.5194/cp-9-1733-2013>.
- Waelbroeck, C., Labeyrie, L., Michel, E., Duplessy, J.C., McManus, J.F., Lambeck, K., Balbon, E., Labracherie, M., 2002. Sea-level and deep water temperature changes derived from benthic foraminifera isotopic records. *Quat. Sci. Rev.* 21, 295–305. [http://dx.doi.org/10.1016/S0277-3791\(01\)00101-9](http://dx.doi.org/10.1016/S0277-3791(01)00101-9).
- Yu, J., Menviel, L., Jin, Z.D., Thornalley, D.J.R., Barker, S., Marino, G., Rohling, E.J., Cai, Y., Zhang, F., Wang, X., Dai, Y., Chen, P., Broecker, W.S., 2016. Sequestration of carbon in the deep Atlantic during the last glacial. *Nat. Geosci.* 9, 319–324. <http://dx.doi.org/10.1038/ngeo2657>.
- Zahn, R., Winn, K., Sarnthein, M., 1986. Benthic foraminiferal $\delta^{13}\text{C}$ and accumulation rates of organic carbon: *Uvigerina peregrina* group and *Cibicides wuellerstorfi*. *Paleoceanography* 1, 27–42.